Solvent Adiabaticity Effects on Ultrafast Electron Transfer in Viologen Charge Transfer Complexes

Andrew M. Moran,† Ponnu Aravindan, and Kenneth G. Spears*

Chemistry Department, Northwestern University, Evanston, Illinois 60208-3113

Received: July 29, 2004; In Final Form: December 23, 2004

Charge recombination (CR) kinetics following photoinduced charge transfer are measured by optical transient absorption for complexes of dimethyl viologen and diheptyl viologen with 4,4′-biphenol (MVBP and HVBP) in methanol. Exponential time constants for MVBP and HVBP are 480 and 790 fs, respectively. Kinetic differences cannot be rationalized with a standard equilibrium nonadiabatic rate formula using parameters obtained from linear absorption and resonance Raman measurements, which give nearly indistinguishable results for the two complexes. Solvent relaxation times and adiabaticities of MVBP are calculated using a full solvation correlation function approach. This analysis suggests that the smaller CR rate of HVBP is due to solvent reorganization differences, and is consistent with a greater adiabatic contribution for HVBP than MVBP. We conjecture that interactions between the diheptyl aliphatic groups of HVBP and the local solvent structure are responsible for the CR differences.

I. Introduction

Standard quantitative descriptions of electron transfer kinetics treat nuclear relaxation as occurring instantaneously on the time scale of the reaction.[1,2] Under equilibrium conditions, the reaction is viewed as a rate process in which underdamped coordinates are cast as quantized accepting modes, whereas the solvent enters as a classical low-frequency bath. However, this model does not hold when nuclear relaxation and reaction rates are comparable. Nuclear relaxation that occurs on the time scale of the reaction may steer a reaction trajectory away from its steepest descent path, resulting in a rate decrease. The extreme case is solvent control of electron transfer in which the rate is solely determined by the longitudinal dielectric relaxation time. Models have been developed for adding adiabatic components to the nonadiabatic electron-transfer rates; the initial work was done by Zusman,[3] and subsequent treatments[1,4−7] have been reviewed by Bixon and Jortner.[2] Solvent control is not common, but it has been found in several systems.[8−12] Electron transfer often is much faster than predicted by solvent control models, and for inverted region electron transfer the solvent is usually treated successfully with standard equilibrium nonadiabatic rate models. The intermediate case of finding clear evidence of solvent relaxation effects on fast nonadiabatic electron transfer is often complicated by the difficulty of isolating the solvent relaxation in various environments without modifying the rate controlling energetic parameters.[13−19] We recently isolated kinetic effects of diffusive solvent relaxation by measuring electron-transfer rates between ion pairs in aqueous solution and in a glassy trehalose−water matrix.[20] Rates were shown to decrease by factors of 2−3 in the glass with respect to solution with only minor differences in absorption and resonance Raman spectra. These systems represent well-defined cases in which kinetic effects are dominated by solvent dynamics and differences in energetic properties are minimal. Diffusive solvent relaxation was rigorously modeled in this work by introducing a diffusive relaxation time and partitioning the solvent reorganization into instantaneous and diffusive components.

Solvent relaxation effects in the inverted region of electron transfer are difficult to study since most environmental changes also create energy shifts in the potential surfaces. While intramolecular charge-transfer systems generally possess better-defined geometries than intermolecular complexes, their processes are more likely to be strongly coupled and to have solvent relaxation components that are coupled to the electronic transition. Weak coupling is desirable because it allows electron transfer to be defined in the nonadiabatic regime. The goal of our work is to probe solvent relaxation effects created by solvation of a substituent not directly involved in the electronic coordinate. This allows comparing CR for two electronically equivalent systems, but with the potential to show solvent relaxation effects. The two intermolecular complexes considered in this work have weakly coupled donor−acceptor sites and reasonably well-defined geometries.

We have selected a well-characterized charge-transfer complex with two different viologen compounds. Spectroscopic and kinetic measurements are presented for charge-transfer complexes (HVBP and MVBP) of diheptyl viologen (HV) and dimethyl viologen (MV) acceptors with the 4,4′-biphenol donor (BP). Structures of each component are shown in Figure 1. Extinction coefficients of the two complexes are identical, and their linear absorption and resonance Raman spectra are almost indistinguishable. However, charge recombination (CR) rates for the transient radical ion pairs created by optically pumping the charge-transfer absorption bands differ by ∼65%; MVBP has the fastest CR rate. These data suggest that nonequilibrium relaxation is responsible for kinetic differences between MVBP and HVBP. The CR rates are sufficiently fast that competing processes such as radical separation, large amplitude nuclear reorganization, and solvent diffusion are negligible.

Geometry changes accompanying oxidation/reduction processes of viologens are well-characterized.[21] Electron delocalization in the viologen radical was shown to be extensive by

* Corresponding author. E-mail: k-spears@northwestern.edu.
† Current address: Chemistry Department, University of Chicago, Chicago, IL 60637.

10.1021/jp0466082 CCC: $30.25
Published on Web 02/15/2005

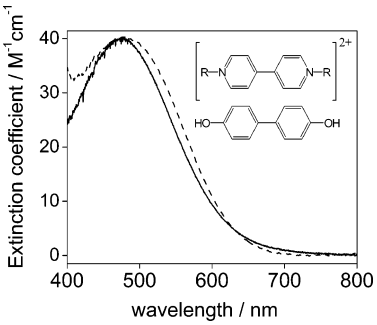

Figure 1. Absorption spectra for complexes of HVBP (dashed) and MVBP (solid). Structures are shown for alkyl viologen (top) and BP (bottom). R is $-CH_3$ and $-(CH_2)_6CH_3$ for MV and HV, respectively.

electron paramagnetic resonance. The *g*-factor of the aryl-substituted viologen is 2.0005,[22] which is close to the value for a free electron (2.002 g). The dihedral angle defining the relative orientation of the aromatic rings in viologen compounds is strongly coupled to the extent of electron delocalization.[23] The angle decreases upon reduction of the dication to form the radical. Measurements made for the 4,4′-bipyridine dication in solution using NMR[24] and anisotropic magnetic susceptibility[25] gave angles of 30° and 37°, respectively. In contrast, the rings of the radical are closer to planarity. Raman and infrared vibrational spectroscopies suggest greater inter-ring C−C bond order for the radical compared to the dication.[26] In a charge-transfer complex with biphenol, the transition density is expected to be localized in the aromatic rings of both components, with a driving force toward a planar complex in the charge-separated state.

While nonadiabatic electron transfer models usually require a quantum model for rate predictions, we are interested in treating solvent dynamics in a model that can include arbitrarily complex solvent relaxation time scales. We omit an explicit sum over vibronic channels in the interest of clarity and investigate a model that uses solvent parameters to create an adiabaticity correction to the nonadiabatic rate. The goal is to compute an effective solvent relaxation time for the CR process in a model for electron transfer.

In this model low-frequency, classically behaved coordinates are most relevant to solvent relaxation effects, and those effects are often described in terms of reaction adiabaticity. Experimental measurements of time-dependent polar solvation dynamics are available to use in describing the solvent relaxation.[27] In activated form, the rate constant, *K*, for electron transfer between states *a* and *b* can be written as[4,5]

$$K = \frac{\sqrt{2\pi}(V^2/\Delta\hbar)\exp(-\delta G^*_{ab}/k_BT)}{1+\sqrt{2\pi}(V^2/\Delta\hbar)[\tau_a+\tau_b]} \quad (1)$$

V is a coupling matrix element, λ_{CM} is the classical reorganization energy,

$$\Delta G^*_{ab} = \frac{(\delta G^0 - \lambda_{CM})^2}{4\lambda_{CM}} \quad (2)$$

is the free energy activation barrier,

$$\Delta^2 = 2\lambda_{CM}k_BT \quad (3)$$

represents the interaction strength between the solute and bath, and τ_a is the solvent relaxation time in state *a*. We note that τ_b can be neglected when thermally activated electron transfer from the ground to the excited state is negligible. There are a variety of ways to parametrize the solvent relaxation time, ranging from simply using the longitudinal dielectric relaxation time[28] to a more rigorous treatment involving the full solvation correlation function.[4,5] The numerator of eq 1 is simply the golden rule expression for reaction rate and the denominator contains the adiabaticity parameter

$$\sqrt{2\pi}(V^2/\Delta\hbar)[\tau_a+\tau_b] \quad (4)$$

which corrects the golden rule expression for bath dynamics that occur on the time scale of the reaction.

II. Experimental and Computational Methods

Kinetic measurements were made by optically pumping the charge-transfer absorption at 490 nm and then monitoring the decay of the viologen radical cation near its peak absorbance of 615 nm.[21] Experiments were carried out using an amplified Ti:sapphire laser system described in a prior publication.[29] The 90 fs output of the compressor is centered at 805 nm with a spectral bandwidth of 22 nm. A laboratory-built near-IR optical parametric amplifier (OPA) was used to generate a 500 nm pump beam (2 μJ/pulse) with a spectral bandwidth of ∼15 nm. Continuum probe pulses were generated by focusing the compressed 800 nm beam into a 3 mm thick piece of optical grade sapphire with a 15 cm focal length lens. Pump and probe beams crossed at an angle of 5° and were focused to spot sizes of 600 and 300 μm, respectively. After the sample, the probe beam was filtered by a short pass interference filter (<750 nm) and coupled into an Ocean Optics spectrograph using an optical fiber. Transient absorption from 400 to 750 nm over a time range of 0 to ∼4 ps was done using alternating pump on/off pulses with electronics and software by Ultrafast Systems Inc.

Raman spectra were recorded using a 532 nm excitation source (Spectra Physics, Millennia Vs) focused to a spot size of <2 mm at the sample. A notch filter (Kaiser Optical Systems) was used to block the laser line. Raman scattering was passed through a polarization scrambler before being focused through a 100 μm slit into a VM-505 single grating monochromator (Acton Research Corporation). The spectrum was dispersed onto a liquid nitrogen cooled CCD detector (Roper Scientific).

The chemicals 1,1′-dimethyl-4,4′-bipyridinium dichloride hydrate, 1,1′-diheptyl-4,4′-bipyridinium dibromide, and 4,4′-biphenol were purchased from Aldrich and used as received. Methanol was purchased from Fischer. Solutions of MVBP and HVBP in methanol were prepared using 1:1 ratios of the components at optical densities of 0.6−0.9 A/mm at the peak of the charge-transfer absorption. Extinction coefficients of MVBP and HVBP (40 ± 5 M^{-1} cm^{-1}) were determined to be identical using the procedure of Rose and Drago.[30] The complex can be studied in methanol at high concentrations, while other common solvents do not have sufficient solubility.

Electronic structure calculations were performed using Gaussian 98 software.[31] Ground-state geometry optimization were performed for BP and the MVBP complex using the B3LYP density functional and 6-311G(d) basis set. In addition, ground-state normal modes were computed for MV and BP. A spherical surface corresponding to a contour of 0.001 esu/bohr^3 was calculated for MVBP using the VOLUME utility of Gaussian 98 at the B3LYP/6-31G(d) level; this corresponds to the suggested cavity radius for Onsager's dielectric continuum model of solvation. The charge is delocalized over the aromatic rings of the dication.

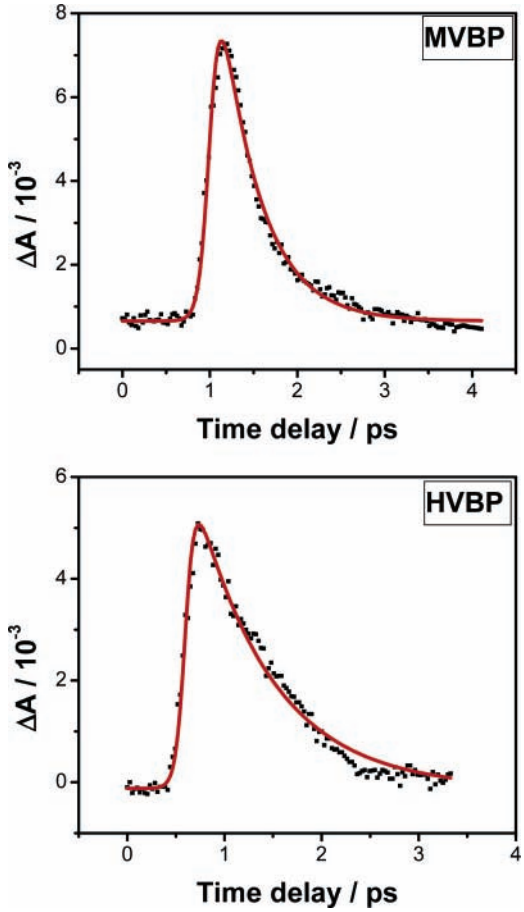

Figure 2. Transient absorption kinetics for MVBP and HVBP. The solid curve (red) is a fitted single exponential of 480 (MVBP) and 790 fs (HVBP). The pump and probe wavelengths are 490 and 615 nm, respectively.

TABLE 1: Kinetic Fitting Parameters

parameter[a]	MVBP	HVBP
decay time/fs[b]	480 ± 40	790 ± 40

[a] The instrument response function is taken to be hyperbolic secant in form with a fwhm parameter of ~200 fs defined by a transient absorption of rhodamine 6G; the peak location depends on wavelength due to dispersion in the system. The variable parameters were the amplitude, excitation peak location, and exponential decay time. [b] The error range is a standard deviation given by averaging 6−7 points over different probe wavelengths and two different experiments. The noise in the individual data points was incorporated in the nonlinear algorithm, which gave a reduced χ^2 value near unity for a single-exponential model.

III. Results

Charge transfer absorption spectra for the two complexes are shown in Figure 1. The peak position of HVBP is slightly red shifted compared to MVBP. Minor differences in line shape are also evident. The charge-transfer spectrum of HVBP overlaps with a higher energy transition localized on the acceptor. The absorption spectrum of MVBP (HVBP) was fit to a Gaussian function over the wavelength range from 410 to 800 nm, giving a peak frequency ω of 21300 cm^{-1} (21275 cm^{-1}) and a width $\delta\omega$ of 5770 cm^{-1} (6435 cm^{-1}).

Transient absorption kinetics are presented in Figure 2 and Table 1. Decays of the radical absorption were fit to an exponential function using a nonlinear least-squares algorithm. The instrument response function, which is a convolution of the pump and probe pulses, was determined by fitting a rhodamine 6G bleach rise time to a hyperbolic secant function. The pulse width parameter (fwhm) is ~200 fs and it depends on the setup conditions. Decay time constants of 480 ± 40 and 790 ± 40 fs were obtained for MVBP and HVBP, respectively. The HVBP decay is 65% longer than that for MVBP.

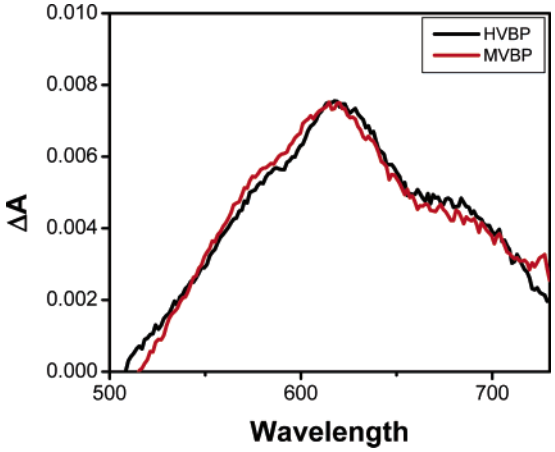

Figure 3. Transient absorption spectra for the MVBP (red) and HVBP (black) radical ions at the time delay for peak absorbance. These spectra are averaged to reduce noise by using 5 time points over a 104 fs interval.

Measurements for both complexes were made three times, and ~7 of the lowest noise transient decays over wavelengths of 580, 600, 615, and 680 nm were averaged to give a standard deviation of 40 fs. The noise level usually is ~0.0002 absorbance units, and the single exponential fit had a reduced χ^2 near unity, which suggests that a single exponential decay is adequate. The fit sometimes appears to show some very small systematic deviations, but statistically over many data sets only a simple exponential form can be fit by these data. The bleach of the charge-transfer transition is not included in the fit because its absorbance is negligible compared to that of the radical (ϵ = 17000 M^{-1} cm^{-1} at 610 nm).[21]

Radical spectra are shown in Figure 3 at a time delay corresponding to peak absorbance. Both spectra peak near 615 nm and are similar to the red of the peak, but for HVBP the spectra is slightly broader on the blue shoulder. However, for HVBP we also had significant excitation light scatter into the transient optical system, which is distorting the region at wavelengths less than 550 nm. This distortion was very obvious on one run (not shown), and is the likely explanation. The spectra also were compared at a 100 fs earlier time and at later times and were very similar; therefore we can conclude that after 150−200 fs delay the electronic states of the MV and HV radical cations are in their final form.

Resonance Raman spectra are presented in Figure 4. Frequencies and intensities are in close agreement with the exception of a transition located at 1174 and 1191 cm^{-1}, for HVBP and MVBP, respectively. The line width of the transition is 15 cm^{-1} greater for HVBP (25 cm^{-1}) than MVBP. This mode is assigned to the C−N stretch of the aliphatic group relative to the aromatic ring, so a reduced frequency for HVBP is sensible. The correspondence in frequency for all other modes suggests that geometries of the donor and acceptor are similar in both complexes. Explicit assignments for all modes are given in Table 2. A comparison of the solvent to solute intensity ratios in a given spectrum can be used to estimate absolute Raman cross sections for transitions of the complex.[32] By considering the 1035 cm^{-1} transition of methanol as an internal standard and normalizing the solute peak areas for concentration ([HVBP]/[MVBP] = 1.7 in Figure 4), we find that the transition cross

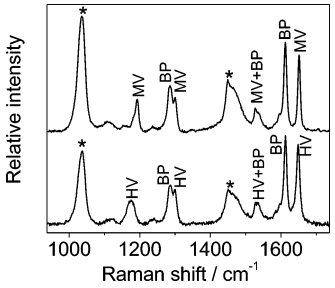

Figure 4. Resonance Raman spectra for MVBP (top) and HVBP (bottom) excited at 532 nm. MV, HV, and BP denote the species responsible for individual transitions. Solvent transitions are labeled by asterisks.

TABLE 2: Vibrational Frequencies and Assignments for Observed Raman Transitions

viologen modes/cm^{-1}			
MV	HV	calcd[a]/cm^{-1}	assignment
1192	1175	1188, 1193[b]	CH_x(aliph.)−N str.
1300	1300	1308	C−C inter-ring, ring def.
1527[c]	1530[c]	1559	C−N str. ring, ring def.
1652	1649	1680	ring sym. str.
biphenol modes/cm^{-1}		calcd[a]/cm^{-1}	assignment
1286		1307	C−C inter-ring
1530[c]		1559	ring def., C−C str. ring
1613		1659	sym. stretch of rings

[a] Calculated for MV at the B3LYP/6-311G(d) level. [b] Modes are too similar to distinguish. [c] This peak possesses contributions from both the donor and acceptor.

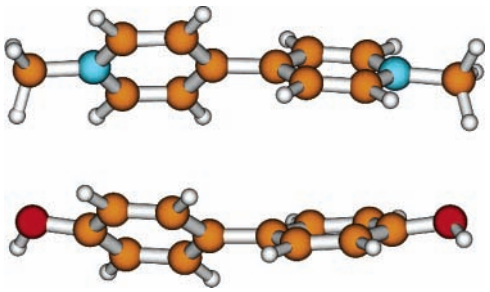

Figure 5. Ground-state equilibrium geometry of MVBP calculated at the B3LYP/6-311G(d) level.

sections differ by less than 10% for all modes besides the 1185 and 1530 cm^{-1} modes, which are also the weakest.

An ab initio ground state geometry optimization of MVBP resulted in the aromatic face-to-face configuration shown in Figure 5. The planes of the rings are separated by ~4.0 Å and the vertices of each ring are configured in a symmetric manner with respect to its face-to-face partner. An intramolecular dihedral angle of 51° defines the relative orientation of rings. Normal-mode analyses of MV and BP were used to describe vibrational modes observed in the Raman spectra (Table 1).

IV. Kinetic Model

In this section, a semiquantitative model of nonequilibrium relaxation is applied to MVBP. The goal is to estimate an effective relaxation time (τ_a in eq 1) for MVBP. First, equilibrium energetic parameters are computed using our measurements and ab initio electronic structure calculations. We then use these parameters to calculate relaxation times for MVBP with empirical solvation correlation functions for methanol.

TABLE 3: Summary of Parameters Derived from Absorption and Raman Spectra

parameter	MVBP	HVBP
ϵ/M^{-1} cm^{-1}	40	40
ω^a/cm^{-1}	21300	21275
$\delta\omega^a$/cm^{-1}	5770	6435
r^b/Å	4.0	4.0
V^c/cm^{-1}	361	381
Δ^d/cm^{-1}	1598	
$\lambda_{CM}{}^e$/cm^{-1}	6162	
R^f/Å	6.02	

[a] Fit to absorption spectra. [b] Distance between donor and acceptor sites. [c] $V = 0.0206r^{-1}(\epsilon\omega\delta\omega)^{1/2}$. [d] Equation 5. [e] Equation 6. [f] A 0.001 esu/bohr^3 electron density contour calculated at the B3LYP/6-31G(d) level.

Parameters of the standard golden-rule formula for electron transfer (numerator of eq 1) can be obtained from our measurements. The electronic coupling V may be estimated using $V = 0.0206r^{-1}(\epsilon\omega\delta\omega)^{1/2}$.[33] At the computed interspecies distance of 4 Å, electronic coupling constants of 361 and 381 cm^{-1} are calculated for MVBP and HVBP, respectively. We assume that r does not differ significantly between complexes because the extinction coefficients, which inherently depend on this distance, and ground-state vibrational frequencies are in close agreement. The solute−solvent coupling Δ (eq 1) is not measured directly but can be obtained in the static limit of line broadening using[34]

$$\Delta^2 = 2\lambda_{CM}k_BT \tag{5}$$

where λ_{CM} is the classical solvent reorganization energy, k_B is Boltzmann's constant, and T is temperature. We calculate λ_{CM} using a spherical reagent model:[34]

$$\lambda_{CM} = \frac{(\mu_e - \mu_g)^2}{4\pi\epsilon_0 R^3}\left[\frac{1}{\epsilon_{op}} - \frac{1}{\epsilon_s}\right] \tag{6}$$

where μ_i represents the static dipole of state i, R is the radius of a cavity centered around the dipole, and ϵ_{op} (ϵ_s) is the optical (static) solvent dielectric constant. The reorganization energy λ_{CM} for MVBP is 6162 cm^{-1} using the ab initio calculated radius (R = 6.02 Å) with a 4 Å distance between donor and acceptor sites. We will assume that λ_{CM} does not differ greatly for HVBP; the premises for this assumption are discussed below. Independent measures of the free energy gaps and intramolecular reorganization energies are not available, but we note the relation between the numerator of eq 1 and the absorption spectrum:[4,5]

$$\sqrt{2\pi}\Delta\sigma(\delta G^0, \lambda_{QM}, \lambda_{CM}) = \exp(-\delta G^*_{ab}/k_BT) \tag{7}$$

where δG^0 is the equilibrium free energy gap, λ_{QM} is the reorganization energy of underdamped intramolecular modes, and $\sigma(\delta G^0,\lambda_{QM},\lambda_{CM})$ is the absorption line shape. The correspondence of the absorption spectra therefore suggests that the energy dependence of δG^*_{ab} is similar for both complexes. A summary of the parameters discussed above is presented in Table 3. We note that the rate formula of eq 1 may also be written with a sum over quantized accepting modes weighted by Franck−Condon factors. With respect to this full quantum treatment, the Raman spectra suggest similarly weighted vibronic channels for both complexes; our measurements show that the absolute scattering cross sections, which are most directly related to the Franck−Condon factors,[32] are similar at a 532 nm excitation wavelength.

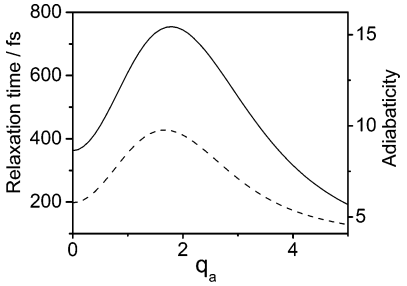

Figure 6. Relaxation times calculated using correlation functions solvation functions $M(t)$ given in refs 27 (solid) and 35 (dashed), respectively. The calculations were performed using eqs 8 and 9.

We next examine the dependence of the adiabaticity on energetic parameters using a full correlation function approach. The relaxation time τ_a is written as[4,5]

$$\tau(q_a) \equiv \exp\left(\frac{-q_a^2}{2}\right)\int_0^\infty \mathrm{d}t\left\{\frac{1}{\sqrt{1-M^2(t)}}\exp\left[\frac{q_a^2 M(t)}{1+M(t)}\right]-1\right\} \tag{8}$$

where $M(t)$ is the solvation correlation function and q_a is given by

$$q_a^2 = \frac{(\delta G^0 + \lambda_{Total})^2}{2\lambda_{Total} k_B T} \tag{9}$$

where $\lambda_{Total} = \lambda_{CM} + \lambda_{QM}$. The strength of this approach is that the correlation function may assume an arbitrary functional form allowing multiple relaxation modes to enter the calculation, whereas parametrizations based on a single dielectric relaxation time generally represent a single-exponential process.

Evaluation of eq 8 requires parametrization of the solvation function $M(t)$. We take the result of Maroncelli,[27] which was determined to be consistent with fluorescence upconversion data for coumarin 153. The function is the sum of four exponentials with coefficients (time constants) of 0.101 (0.030 ps), 0.340 (0.28 ps), 0.298 (3.20 ps), and 0.261 (15.3 ps). The result for MVBP using the parameters in Table 3 is presented in Figure 6. The relaxation time varies by less than a factor of ~2.5 over the entire reasonable range of q_a. Conservatively, the realistic values of q_a are likely to be in the interval between 1 and 4, which correspond to λ_{QM} of 3489 and 1036 cm^{-1}, respectively (the relation $\omega = -\delta G^0 + \lambda_{Total}$ was used here with λ_{CM} from Table 3 of 6162 cm^{-1}). These cases cover a range of δG^0 from −11650 to −14100 cm^{-1}, respectively. Adiabaticities also were calculated using a simpler bimodal form of the correlation function with a 30 fs Gaussian decay and 500 fs exponential decay that comprise 20% and 80% of the amplitude, respectively.[35] This result is shown in Figure 6, and has a similar form and faster relaxation at the peak. For methanol the longitudinal relaxation time calculated from dielectric dispersion data[27] is dominated by the fastest component of ~4.4 ps, and results in adiabaticities that are more than three times greater than the result found using Maroncelli's parameters. [27]

Absolute rate values for a nonadiabatic quantum model of rate transfer are difficult to predict, and we do not have sufficient data on this charge-transfer complex to make an accurate calculation and comparison to our data. Specifically, the δG^0 and λ_{QM} are not known. However, the parameters defined above allow us to compute rates for a realistic range of free energy and internal reorganization energy. The range of adiabaticity in Figure 6 applied to eq 1 suggests that intrinsic absolute electron-transfer rate (numerator of eq 1) would be larger than the measured rate by 3−15 times, depending on the value of q_a.

The importance of Figure 6 is to identify a range of solvent relaxation times for MVBP, which sets a scale for the increased relaxation time of HVBP consistent with its longer CR decay of 790 fs.

V. Discussion

The main conclusion of this article is that the 65% smaller CR rate for HVBP than MVBP is not expected from the supporting spectroscopic evidence, which predicts essentially the same CR rate for both. The structure of the HVBP complex was selected to create solvent perturbation without being intimately involved in the charge transfer transition. Three possible objections to the expectation of equal CR rates include concern about the similarity of the intra-complex geometries, concern about a slightly broader linear absorption spectrum in the case of HVBP, and concern about a UV electronic transition that slightly overlaps the charge-transfer band in HVBP but not MVBP.

We now address these issues individually. First, we have put forth three independent arguments in favor of structural similarity between the two complexes: (i) absorption spectra are very similar with identical extinction coefficients (the relation to electronic coupling was discussed in the previous section); (ii) resonance Raman spectra have similar frequencies and intensities, which represent similar ground state geometries and charge redistribution in the excited state, respectively; and (iii) ab initio geometry optimization of MVBP converges to a stable structure in which the attractive force is face-to-face interaction between aromatic rings, and the same forces are present in HVBP. Second, small inhomogeneity in the complex structure may contribute to the greater line width of HVBP. However, an inhomogeneous distribution enters the rate formula outside the golden rule expression; the observed charge-transfer rate may be calculated as a simple sum over a distribution of rate constants weighted by probabilities. Inhomogeneity does not necessarily give slower rates, but could affect the decay profile; however, the quality of fit to an exponential form is very similar for both HVBP and MVBP. The transient absorbance in Figure 3 shows only slight differences between the HV radical cation and the MV radical cation. These spectra are stable in time from about 100 fs before the peak (~200 fs response function) to longer times, and the kinetic traces at wavelengths from 580 to 680 nm are identical. Any significant inhomogeneous effects should show up in the kinetics across this spectral range. Third, the effect of the overlapping UV electronic transition in HVBP is likely to be minor if it contributes at all. The charge-transfer transition was pumped at 480−490 nm, a spectral region where the absorbance of this transition is weak. Furthermore, decay of the radical absorption was monitored at many wavelengths ranging from 580 to 680 nm, where the UV transition does not absorb.

Taken together, the linear absorption spectra, transient spectra, resonance Raman spectra, and electronic structure calculations constitute a strong argument for the isolation of a nonequilibrium solvent effect on charge recombination kinetics. The charge-transfer absorption spectra of the complexes are not significantly shifted in frequency or peak extinction coefficient, so it is unlikely that the aliphatic chains are in close proximity to the aromatic rings. In addition, the transient spectrum of the viologen radical does not show short-time spectral shifts or wavelength-dependent kinetics, which implies that rapid polar

solvation is similar for both complexes. *The assumption of similar λ_{CM} for MVBP and HVBP is based on these premises.* The next step is to identify a reasonable conjecture for the solvent relaxation mechanism.

The concept of time-scales in solvation processes has been previously discussed in many contexts; for example, Berg's viscoelastic model[36] of nonpolar solvation predicts that diffusive solvent structural relaxation is dominant after 500 fs, whereas the time interval from 100 to 500 fs is described as collective and inertial (viscosity-independent). The diffusive time-scale $\geq$500 fs is related to relaxation of solvent structure, whereas at shorter times local potential energy distributions are preserved, allowing the inertial regime to be described using instantaneous normal modes.[37] Simulations of solvation dynamics demonstrate the importance of ultrafast inertial response and the difficulty of making a clean separation of dielectric and mechanical friction effects.[38,39] In the model of electron transfer used in this work the solvent relaxation time scale must be comparable to the reaction rate to affect the adiabaticity, which we have shown is valid for these systems.

We propose a microscopic picture in which two types of solute−solvent interactions are considered: (i) polar solvation of the aromatic rings by methanol molecules and (ii) nonpolar interaction between the aliphatic chains and the surrounding solvent structure. For these systems, polar solvation is certainly important since charge reorganization occurs in the aromatic rings of both components upon excitation. As discussed above, the evidence is for similar energetics in both MVBP and HVBP. Therefore, we ascribe differences in the CR rate to the effect of nonpolar interaction between the aliphatic groups and the solvent. However, the identity of this interaction is not easily deduced since the relevant interactions are not affecting the solute optical properties.

As stated in the Introduction, it is generally accepted that the dihedral angle between the aromatic rings of viologens decreases in the +1 oxidation state compared to the +2 state.[21] Motion of this coordinate toward planarity should be very fast, and we see no evidence for spectral differences between MVBP and HVBP in the rise time region of their transients at a delay of 150−200 fs. The dihedral angle change must involve small amplitude collective motion of methanol near the aromatic rings, and should be similar for MVBP and HVBP.

Our measurements do not allow for precise parametrization of the solvation function $M(t)$, nor do they directly reveal the nuclear motion associated with the difference between MVBP and HVBP. The model that we used allows examination of different solvation functions and predicts a solvent relaxation time that can be interpreted in terms of the adiabaticity of charge recombination. However, the understanding of electron transfer in terms of adiabaticity for these ultrafast processes is probably an oversimplification of a complex solvent relaxation process. A molecular dynamics simulation is required to give a more detailed conceptual picture and these complexes might be a good candidate for such models. Further experimental work in other solvents without hydrogen bonding and different types of hydrogen bonding will be needed to develop more insights into how solvent structure might be operating in this system.

In conclusion, our spectroscopic measurements show that the MVBP and HVBP charge-transfer complexes possess similar parameters with respect to the standard nonadiabatic electron-transfer rate predictions, and should have had similar charge recombination rates. The 65% slower CR rate of HVBP (790 fs) than MVBP (480 fs) was interpreted as a nonequilibrium solvent relaxation effect that is consistent with a greater adiabatic contribution for HVBP than MVBP. The full correlation function approach to the calculation of solvent relaxation times predicts that relaxation time scales are on the same scale as the electron-transfer times. These complexes illustrate how molecular structures can be selected to show solvation relaxation effects on ultrafast electron transfer.

Acknowledgment. This work was supported by the U.S. Department of Energy, Office of Science (Grant DE-FG02-91ER14228). We thank R. P. Van Duyne for use of his Raman apparatus.

References and Notes

(1) Sumi, H.; Marcus, R. A. *J. Chem. Phys.* **1986**, *84*, 4894.
(2) Bixon, M.; Jortner, J. Electron Transfer−From Isolated Molecules to Biomolecules. In *Advances in Chemical Physics*; Rice, S. A., Ed.; John Wiley and Sons: New York, 1999; Vol. 106.
(3) Zusman, L. D. *Chem. Phys.* **1980**, *49*, 295.
(4) Sparpaglione, M.; Mukamel, S. *J. Chem. Phys.* **1988**, *88*, 3263.
(5) Sparpaglione, M.; Mukamel, S. *J. Chem. Phys.* **1988**, *88*, 4300.
(6) Hynes, J. T. *J. Phys. Chem.* **1986**, *90*, 3701.
(7) McManis, G. E.; Weaver, M. J. *J. Chem. Phys.* **1989**, *90*, 912.
(8) Tominaga, K.; Walker, G. C.; Kang, T. J.; Barbara, P. F.; Fonseca, T. *J. Phys. Chem.* **1991**, *95*, 10485.
(9) Kang, T. J.; Kahlow, M. A.; Giser, D.; Swallen, S.; Nagarajan, V.; Jarzeba, W.; Barbara, P. F. *J. Phys. Chem.* **1988**, *92*, 6800.
(10) Horng, M. L.; Dahl, K.; Jones, G., II; Maroncelli, M. *Chem. Phys. Lett.* **1999**, *315*, 363.
(11) Heitele, H. *Angew. Chem., Int. Ed. Engl.* **1993**, *32*, 359.
(12) Kosower, E. M.; Huppert, D. *Annu. Rev. Phys. Chem.* **1986**, 127.
(13) Akesson, E.; Johnson, A. E.; Levinger, N. E.; Walker, G. C.; DeBruil, T. P.; Barbara, P. F. *J. Chem. Phys.* **1992**, *96*, 7859.
(14) Haberle, T.; Hirsch, J.; Pollinger, F.; Heitele, H.; Michel-Beyerle, M. E.; Staab, H. A. *J. Phys. Chem.* **1996**, *100*, 18269.
(15) Kobayashi, T.; Takagi, Y.; Kandori, H.; Kemnitz, K.; Yoshihara, K. *Chem. Phys. Lett.* **1991**, *180*, 416.
(16) Pal, H.; Nagasawa, Y.; Tominaga, K.; Yoshihara, K. *J. Phys. Chem.* **1996**, *100*, 11964.
(17) Sinks, L. E.; Wasielewski, M. R. *J. Phys. Chem. A* **2003**, *107*, 611.
(18) Wiederrecht, G. P.; Svec, W. A.; Wasielewski, M. R. *J. Phys. Chem. B* **1999**, *103*, 1386.
(19) Tominaga, K.; Kliner, D. A. V.; Johnson, A. E.; Levinger, N. E.; Barbara, P. F. *J. Chem. Phys.* **1993**, *98*, 1228.
(20) Moran, A. M.; Spears, K. G. *Chem. Phys. Lett.* **2004**, *393*, 397.
(21) Monk, P. M. S. *The Viologens*: *Physiochemical Properties, Synthesis and Applications of the Salts of 4,4′-Bipyridine*; John Wiley and Sons: New York, 1998.
(22) Yoon, K. B.; Kochi, J. K. *J. Am. Chem. Soc.* **1989**, *111*, 1128.
(23) Hofmann, H. J.; Cimiraglia, R.; Tomasi, J. *J. Mol. Struct.* **1986**, *169*, 213.
(24) Emsley, J. W.; Stephenson, D. S.; Lindon, J. C.; Lunazzi, L.; Pulga, S. *J. Chem. Soc.* **1975**, *2*, 1541.
(25) Timosheva, A. P.; Kushnikovskii, I. A.; Vul'Fson, S. G.; Vereshchagin, A. N. *Bull. Acad. Sci. USSR* **1991**, *40*, 2771.
(26) Hester, R. E.; Suzuki, S. *J. Phys. Chem.* **1982**, *86*, 4626.
(27) Horng, M. L.; Gardecki, J. A.; Papazyan, A.; Maroncelli, M. *J. Phys. Chem.* **1995**, *99*, 17311.
(28) Marcus, R. A. *Understanding Molecular Properties*; Avery, J., Ed.; D. Reidel Publishing Co.: Dordrecht, The Netherlands, 1987; p 229.
(29) Marin, T. W.; Homoelle, B. J.; Spears, K. G.; Hupp, J. T.; Spreer, L. O. *J. Phys. Chem. A* **2002**, 1131.
(30) Rose, N. J.; Drago, R. S. *J. Am. Chem. Soc.* **1959**, *81*, 6138.
(31) Frisch, M. J.; Trucks, G. W.; Schlegel, H. B.; Scuseria, G. E.; Robb, M. A.; Cheeseman, J. R.; Zakrzewski, V. G.; Montgomery, J. A., Jr.; Stratmann, R. E.; Burant, J. C.; Dapprich, S.; Millam, J. M.; Daniels, A. D.; Kudin, K. N.; Strain, M. C.; Farkas, O.; Tomasi, J.; Barone, V.; Cossi, M.; Cammi, R.; Mennucci, B.; Pomelli, C.; Adamo, C.; Clifford, S.; Ochterski, J.; Petersson, G. A.; Ayala, P. Y.; Cui, Q.; Morokuma, K.; Malick, D. K.; Rabuck, A. D.; Raghavachari, K.; Foresman, J. B.; Cioslowski, J.; Ortiz, J. V.; Stefanov, B. B.; Liu, G.; Liashenko, A.; Piskorz, P.; Komaromi, I.; Gomperts, R.; Martin, R. L.; Fox, D. J.; Keith, T.; Al-Laham, M. A.; Peng, C. Y.; Nanayakkara, A.; Gonzalez, C.; Challacombe, M.; Gill, P. M. W.; Johnson, B. G.; Chen, W.; Wong, M. W.; Andres, J. L.; Head-Gordon, M.; Replogle, E. S.; Pople, J. A. *GAUSSIAN 98*, Revison A.11.4; Gaussian Inc.: Pittsburgh, PA, 1998.

(32) Myers, A. B. *Chem. Rev.* **1996**, *96*, 911.
(33) Hush, N. S. *Prog. Inorg. Chem.* **1967**, *8*, 391.
(34) Mukamel, S. *Principles of Nonlinear Optical Spectroscopy*; Oxford University Press: Oxford, UK, 1995.
(35) Fonseca, T.; Ladanyi, B. M. *J. Phys. Chem.* **1991**, *95*, 2116.
(36) Berg, M. A. *J. Phys. Chem. A* **1998**, *102*, 17.
(37) Buchner, M.; Ladanyi, B. M.; Stratt, R. M. *J. Chem. Phys.* **1992**, *97*, 8522.
(38) Kumar, P. V.; Maroncelli, M. *J. Chem. Phys.* **2000**, *112*, 5370.
(39) Ladanyi, B. M.; Maroncelli, M. *J. Chem. Phys.* **1998**, *109*, 3204.